

Revealing Novel Aspects of Light-Matter Coupling by Terahertz Two-Dimensional Coherent Spectroscopy: The Case of the Amplitude Mode in Superconductors

Kota Katsumi^{1,*}, Jacopo Fiore², Mattia Udina², Ralph Romero III¹, David Barbalas¹, John Jesudasan³,
Pratap Raychaudhuri³, Goetz Seibold⁴, Lara Benfatto² and N. P. Armitage¹

¹*William H. Miller III, Department of Physics and Astronomy, The Johns Hopkins University, Baltimore, Maryland 21218, USA*

²*Department of Physics and ISC-CNR, Sapienza University of Rome, Piazza le A. Moro 5, 00185 Rome, Italy*

³*Department of Condensed Matter and Material Science, Tata Institute of Fundamental Research, Homi Bhabha Road, Colaba, Mumbai 400005, India*

⁴*Institut für Physik, BTU Cottbus-Senftenberg, P.O. Box 101344, 03013 Cottbus, Germany*



(Received 19 November 2023; revised 4 March 2024; accepted 17 May 2024; published 21 June 2024)

Recently developed terahertz (THz) two-dimensional coherent spectroscopy (2DCS) is a powerful technique to obtain materials information in a fashion qualitatively different from other spectroscopies. Here, we utilized THz 2DCS to investigate the THz nonlinear response of conventional superconductor NbN. Using broadband THz pulses as light sources, we observed a third-order nonlinear signal whose spectral components are peaked at twice the superconducting gap energy 2Δ . With narrow-band THz pulses, a THz nonlinear signal was identified at the driving frequency Ω and exhibited a resonant enhancement at temperature when $\Omega = 2\Delta$. General theoretical considerations show that such a resonance can arise only from a disorder-activated paramagnetic coupling between the light and the electronic current. This proves that the nonlinear THz response can access processes distinct from the diamagnetic Raman-like density fluctuations, which are believed to dominate the nonlinear response at optical frequencies in metals. Our numerical simulations reveal that, even for a small amount of disorder, the $\Omega = 2\Delta$ resonance is dominated by the superconducting amplitude mode over the entire investigated disorder range. This is in contrast to other resonances, whose amplitude-mode contribution depends on disorder. Our findings demonstrate the unique ability of THz 2DCS to explore collective excitations inaccessible in other spectroscopies.

DOI: [10.1103/PhysRevLett.132.256903](https://doi.org/10.1103/PhysRevLett.132.256903)

A transition to a state of matter that spontaneously breaks a continuous U(1) symmetry of the Hamiltonian is characterized by the emergence of collective electronic modes associated with amplitude and phase fluctuations of the complex order parameter [1,2]. The finite energy amplitude mode is an analog of the Higgs boson associated with the electroweak symmetry breaking of the fundamental vacuum [1,2]. In condensed matter physics, amplitude modes have been explored in various ordered phases, such as charge density waves (CDWs) [3–6], antiferromagnets [7–9], and superfluid ^3He [10,11]. In the case of superconductors, long-range Coulomb interaction pushes the otherwise massless phase mode up to the plasma frequency, while the amplitude mode stays intact at twice the superconducting (SC) gap energy 2Δ [1,2]. The observation of the amplitude mode in superconductors is challenging, because it does not couple linearly to light being charge neutral, and it is expected to have a weak Raman response [12–14] in cases when spontaneous Raman scattering can be interpreted as a probe of density fluctuations [15]. An exception is the case of $2H\text{-NbSe}_2$ [16–20] or $2H\text{-TaS}_2$ [21], where superconductivity coexists with CDW order and the amplitude mode can be seen in Raman

spectroscopy by virtue of its coupling to the Raman-active soft CDW phonon [20,22].

With the aim of identifying the amplitude mode in superconductors, the terahertz (THz) nonlinear optical response has been explored. THz nonlinear responses, such as pump-probe response or third-harmonic generation (THG) in a conventional superconductor NbN, have been initially interpreted as the excitation of an amplitude mode through a nonlinear coupling to the electromagnetic field [2,23–26]. Since then, the THz nonlinear response has been extensively explored in superconductors like MgB_2 [27–29], high-temperature cuprates [30–34], and iron-based systems [35–39]. Motivated by these experiments, theoretical works have shown that the third-harmonic (TH) THz nonlinear response is governed by quasiparticle excitations as well as the amplitude mode, with a relative hierarchy of the two contributions that depends on the disorder level and pairing strength [12,13,40–47]. Importantly, theoretical considerations highlighted the possibility that THz nonlinearities can be mediated by an intrinsically different electronic response as compared to conventional nonlinearities at optical frequencies of a few eV [13,42,44]. In principle, the latter is governed by

diamagnetic Raman-like density-density scattering in metals [15], whereas even weak disorder may allow THz light to trigger paramagnetic current-current fluctuations. Nevertheless, clear experimental indication of the predominance of paramagnetic processes has not been reported.

Toward this aim, the recently developed multidimensional coherent spectroscopy is promising, as it may allow one to disentangle different nonlinear processes [48]. In the case of THz two-dimensional coherent spectroscopy (2DCS), magnon [49], phonon [50], plasmon [51], and electronic excitations in disordered systems [52] have been clearly identified. In this Letter, we investigated the THz nonlinear response of the dirty-limit conventional superconductor NbN by THz 2DCS. Using broadband THz, we observed a nonlinear signal peaked at twice the SC gap energy 2Δ . As the temperature increases, this nonlinear signal's peak exhibits a redshift following the temperature dependence of 2Δ obtained from the equilibrium optical response. To resolve the origin of these nonlinear spectral features, we employed narrow-band THz pulses at the driving angular frequency $\Omega/2\pi = 0.63$ THz for THz 2DCS. We identified a first-harmonic (FH) nonlinear signal whose intensity displays a resonant enhancement when 2Δ matches the driving frequency Ω . General theoretical considerations show that this FH signal, inaccessible in previous works focusing on THG, can be generated only by the aforementioned paramagnetic processes. Our numerical simulations demonstrate that, with finite disorder, the $\Omega = 2\Delta$ resonance of the FH response is dominated by the amplitude mode, offering a preferential route for its detection.

The schematic of the experiment is depicted in Fig. 1(a). Two intense single-cycle (broadband) THz pulses are generated using the tilted-pulse front technique with LiNbO₃ [53–55]. See Supplemental Material [56] for details. We first performed THz 2DCS on NbN ($T_c = 14.9$ K) using broadband THz pulses. The peak E field of A and B pulses did not exceed 3 kV/cm to avoid the depletion of the SC condensate. We measured the transmitted THz E fields of two pulses [$E_A(t, \tau)$ and $E_B(t)$] separately and of both pulses [$E_{AB}(t, \tau)$] together as shown in Fig. 1(b). We swept the delay time τ of the A pulse with respect to the arrival of the B pulse. The nonlinear signal's E field is obtained as $E_{NL}(t, \tau) = E_{AB}(t, \tau) - E_A(t, \tau) - E_B(t)$, presented in Fig. 1(c). We perform a Fourier transform with respect to t or both t and τ . Figure 1(d) shows the power spectrum of the nonlinear signal at 5 K when $\tau = 0$ ps (the purple curve). The nonlinear signal exhibits two peaks: One matches twice the SC gap 2Δ identified in the THz optical conductivity measured at 5 K (the green curve on the right axis), and the other is located at slightly higher energy than the center frequency of the B pulse.

In Fig. 2(a), we present the power spectrum of the nonlinear signal at $\tau = 0$ ps measured at different temperatures. The peak energy in the nonlinear signal shows a

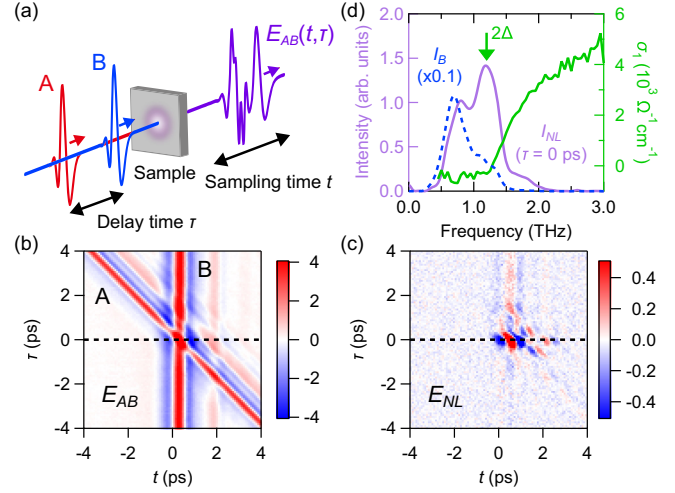


FIG. 1. (a) A schematic of the THz 2DCS experiment. (b) Time traces of the A and B pulses together [$E_{AB}(t, \tau)$] transmitted after the NbN sample ($T_c = 14.9$ K) at 5 K as a function of the sampling time t and the delay time τ . (c) The same plot as (b) but for the nonlinear signal $E_{NL}(t, \tau)$. (d) Power spectrum of the THz nonlinear signal from NbN at 5 K measured at $\tau = 0$ ps with the broadband THz pulses (purple, left axis). The blue dashed curve on the left axis is the power spectrum of the B pulse. The green curve on the right axis shows the real part of the optical conductivity at 5 K.

redshift with increasing temperature. We evaluated the energy of the peak in two ways. First, we fit the power spectra of the nonlinear signal using the power spectrum of the B pulse multiplied by a Lorentzian. The fits reasonably reproduce the data as presented by the gray dashed curves in Fig. 2(a). The extracted peak energy is plotted as a function of temperature by red open squares in Fig. 2(c), in good agreement with the temperature dependence of 2Δ (the gray circles) as seen in the linear responses. We also evaluated the peak energy by normalizing the nonlinear signal spectra with the B -pulse spectra, as shown in Fig. 2(b). While the normalized spectra display an increasing tendency toward higher frequency below 12 K, likely due to the THG signal, peaks are discerned in the frequency range from 0.3 to 1.4 THz. We fit the normalized spectrum with a Lorentzian and plot the obtained peak energy as a function of temperature by green open diamonds in Fig. 2(c), consistent with those in the first procedure. We note that the same result of the peak-energy shift is obtained using the A pulse to normalize the nonlinear signal, as shown in Fig. S2 in Supplemental Material [56]. This direct correspondence between the peak energy of the nonlinear signal and the SC gap energy was also found in other NbN samples with different T_c , as presented in Fig. S7 in Supplemental Material [56].

To obtain deeper insight into the spectrum of the nonlinear signal, we performed THz 2DCS using narrow-band THz pulses with the peak E field of 3 kV/cm and a driving angular frequency of $\Omega/2\pi = 0.63$ THz. Figure 3(a) shows

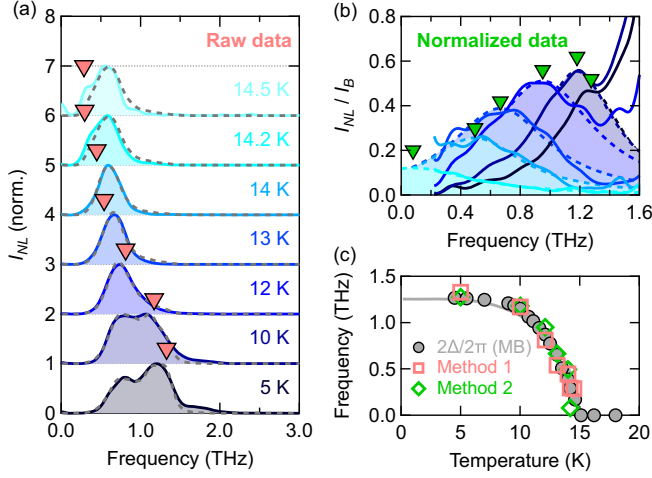


FIG. 2. (a) Power spectrum of the nonlinear signal from NbN ($T_c = 14.9$ K) when $\tau = 0$ ps at different temperatures with single-cycle THz pulses. The gray dashed curves denote the fit to the data using a Lorentzian multiplied by the B -pulse power spectra. The obtained peak energy is presented by the red arrows. (b) The nonlinear signal in (a) divided by the B -pulse power spectra as a function of temperature. The obtained peak energy with fitting is shown by the green arrows. The dashed curves are the fits to the data using a Lorentzian. (c) Peak energy of the nonlinear signal as a function of temperature obtained by fitting the raw data in (a) (red open squares) and the normalized data in (b) (green open diamonds). The gray circles are the temperature dependence of the gap evaluated using the Mattis-Bardeen model.

the nonlinear signal spectra for NbN with $T_c = 14.9$ K measured at 5 K when $\tau = 0$ ps. The power spectrum exhibits two peaks at 0.63 and 1.9 THz, corresponding to the FH and TH contributions, respectively. Both FH and TH intensities follow E^6 as shown in Fig. 3(b) up to the THz peak E field of 10 and 3 kV/cm, respectively, indicating that both are third-order nonlinear responses. In the third-order processes driven at a frequency Ω , the nonlinear signals are generated at frequencies of $\pm\Omega \pm \Omega \pm \Omega$ [65], giving signals at Ω and 3Ω .

Figure 3(c) shows the frequency-integrated intensity of the FH and TH signals as a function of temperature with the multicycle THz pulses when $\tau = 0$ ps. Here, we integrate from 0.3 to 1 THz for the FH signal and from 1.6 to 2.2 THz for the TH signal. The temperature dependence of the TH signal is consistent with the previous reports where it takes its maximum intensity when *twice* the drive frequency matches twice the SC gap energy 2Δ (i.e., $2\Omega = 2\Delta$) as shown in the top panel [2,23,24,26]. By contrast, the FH signal displays a resonant enhancement when the driving frequency matches 2Δ (i.e., $\Omega = 2\Delta$). These behaviors were found in the other NbN samples with different T_c , as shown in Fig. S8 in Supplemental Material [56]. This FH signal has been overlooked in previous THz nonlinear experiments, because it is usually overwhelmed by the transmitted E field at the FH primarily from linear transmission, as shown in Supplemental Material [56]. The

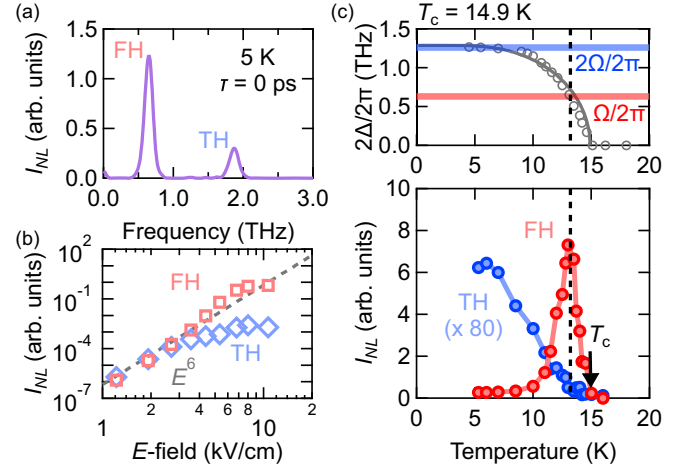


FIG. 3. (a) Power spectrum of the THz nonlinear signal at 5 K measured at $\tau = 0$ ps with narrow-band THz pulses. (b) The frequency-integrated intensity of the FH and TH contributions at 5 K when $\tau = 0$ ps as a function of the B -pulse peak E field. The dashed gray curve is a guide to the eye with a slope of 6. (c) Temperature dependence of the frequency-integrated intensity of the FH (red) and TH (blue) contributions. The top presents the temperature dependence of 2Δ evaluated from the linear conductivity as compared to Ω (red) and 2Ω (blue). The solid gray curve is the gap computed by numerically solving the BCS equation. The black dashed line denotes the temperature that satisfies $\Omega = 2\Delta$.

difference-signal analysis inherent to 2DCS allows it to be unambiguously isolated here.

To clarify the experimental observations, we analyze the different nonlinear processes following the diagrammatic approach in previous works [12,42–44]. The nonlinear processes in the SC state can be obtained by combining the diamagnetic (quadratic) and paramagnetic (linear) couplings between electronic excitation and the electromagnetic field. In the diagrammatic representation, the former is represented as a densitylike electronic vertex with two-photon lines attached, while the latter appears as currentlike electronic vertex with a single-photon line. The third-order nonlinear current is generally expressed as $J_{\text{NL}}(\omega) = \int d\omega_1 d\omega_2 d\omega_3 \delta(\omega_1 + \omega_2 + \omega_3 - \omega) A(\omega_1) A(\omega_2) A(\omega_3) K(\omega_1, \omega_2, \omega_3)$, where $A(\omega)$ denotes the gauge field. Assuming monochromatic fields ($\omega_i = \pm\Omega$ for $i = 1, 2, 3$), the possible combinations of ω_i give peaks at $\omega = \Omega$ and $\omega = 3\Omega$ in $J_{\text{NL}}(\omega)$. The spectral structure simplifies in the clean limit, when only diamagnetic processes are allowed [12]. Because diamagnetic vertices have two-photon lines attached, the nonlinear kernel K can be reduced to $K^{\text{dia}}(\omega_1 + \omega_2)$ and its frequency permutations. Given that the quasiparticles and amplitude-mode fluctuations are both enhanced at 2Δ , both the FH and TH diamagnetic responses are largest when $\omega_1 + \omega_2 = 2\Delta$, and, thus, for single-frequency driving at Ω , their resonance occurs at $\Omega = \Delta$ [12,56].

In contrast, when a finite amount of disorder is included, paramagnetic processes become allowed. Consequently, as detailed in Supplemental Material [56], the nonlinear kernel is a function $K^{\text{para}}(\omega_1, \omega_1 + \omega_2, \omega_1 + \omega_2 + \omega_3)$, plus permutations of the running frequencies, and one expects an enhancement whenever any of the three arguments of K^{para} matches 2Δ . Therefore, unlike the resonance at $\Omega = \Delta$ for the FH and TH responses, the FH response at $\Omega = 2\Delta$ and TH responses at $3\Omega = 2\Delta$ (i.e., $\Omega = 2\Delta/3$) and $\Omega = 2\Delta$ can arise only via paramagnetic processes. They are absent in the usual description of the spontaneous nonresonant Raman at optical frequencies, based on the widely used effective-mass approximation which maps the Raman response into a diamagneticlike susceptibility [15]. We note that the same paradigm does not necessarily apply to the resonant Raman case, leaving open, e.g., the interpretation of recent nonequilibrium anti-Stokes Raman measurements in cuprate superconductors [66].

We examined these expectations by numerical simulations using the attractive Hubbard model on a square lattice with Anderson-type impurities. Following the approach in Refs. [44,46], we computed the nonlinear TH and FH signals, as shown in Figs. 4(a) and 4(b), respectively. Here, we set the disorder level to $k_F l = 10$ (k_F is the Fermi wave vector and l is the electronic mean free path) and evaluated the BCS-quasiparticle contribution (the dashed curves, denoted as BCS) and the sum of it and the amplitude-mode contribution (the solid curves, denoted as BCS + AM) separately (see Supplemental Material [56] for details). For the TH signal, the nonlinear current is enhanced at the expected three possible frequency combinations, as denoted by the vertical arrows in Fig. 4(a). In Supplemental Material [56], we show that the relative ratio between the BCS and amplitude-mode contributions for the lower two peaks is consistent with previous reports [42–44], where the amplitude mode acquires considerable spectral weight for very strong disorder. On the other hand, as shown in Fig. S13 [56], we find that the upper peak at $\Omega = 2\Delta$ is dominated by the amplitude mode for $k_F l = 3, 6, 10$, and 30 , which are relevant to the estimated disorder level of NbN [67,68] summarized in Fig. S12 [56]. The FH $J_{\text{NL}}(\Omega)$ has two features that correspond to the two allowed frequencies for the FH response as discussed above. Again, the amplitude mode dominates the upper resonance for all disorder levels investigated, whereas the lower energy resonance shows appreciable disorder dependence. We note that the dominance of the amplitude mode at $\Omega = 2\Delta$ in both TH and FH responses is an empirical observation from our numerics. The reason for it is a topic of current investigation.

Next, we compute the temperature dependence of the FH and TH signals at $\Omega/2\pi = 0.63$ THz by modeling the kernel resonances numerically, using the temperature dependence of the SC gap obtained from the linear

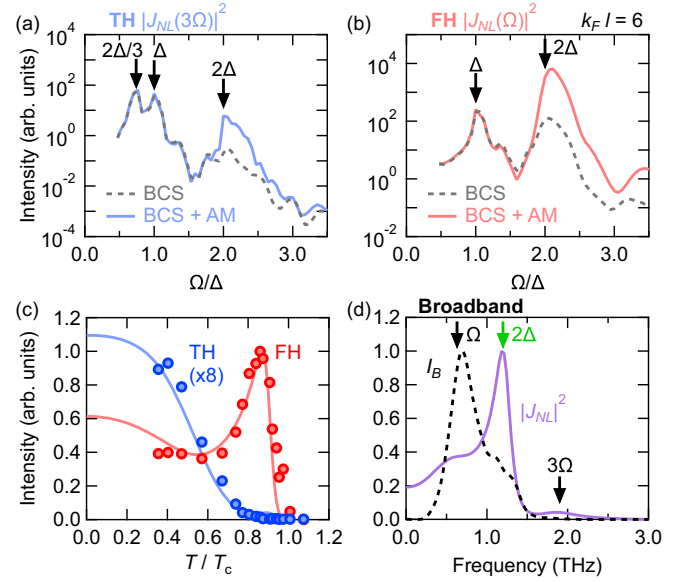


FIG. 4. (a),(b) Nonlinear current intensity $|J_{\text{NL}}|^2$ for the (a) TH and (b) FH components as a function of the driving frequency Ω normalized by the SC gap Δ for the BCS contribution (dashed curve) and the sum of the BCS and amplitude-mode contributions (solid curves). (c) Comparison between the experimental data (open circles) and the theoretical results (solid curves) for the temperature dependence of the FH (red) and TH (blue). The temperature T is normalized by T_c . To remove the temperature-dependent screening effects, the experimental nonlinear signal intensity ($|J_{\text{NL}}|^2$) is normalized by the internal B -pulse E field (E_B^6) (see Ref. [56]). The theoretical results correspond to the nonlinear current intensity $|J_{\text{NL}}|^2$ at the driving frequency of 0.63 THz for an E -field constant in temperature. (d) The nonlinear current simulated using the broadband THz pulses. The black dashed curve shows the intensity of the driving THz E field, obtained by simulating the experimental THz B pulse.

responses (see Supplemental Material [56]). Figure 4(c) compares the numerical results with the experimental data normalized by the incoming THz E field for the FH and TH components. The calculated result for the FH component displays excellent agreement with experiments, unambiguously indicating that the FH signal stems from the amplitude-mode contribution at $\Omega = 2\Delta$ via the paramagnetic processes. The numerical result for the TH component displays a monotonic increase when the temperature is lowered, consistent with the experimental data. The increase in the TH intensity toward the lower temperature is due to the resonance of $\Omega = \Delta$ around 0 K, which is likely dominated by the amplitude mode in the high disorder level relevant for NbN. To check the internal consistency of our approach, we further simulate the nonlinear current driven by broadband THz pulses (see Supplemental Material [56] for details). Figure 4(d) presents the nonlinear current induced by the broadband THz pulses for $2\Delta/2\pi = 1.2$ THz. The computed nonlinear current exhibits three peaks at $\Omega/2\pi = 0.63$ THz,

$2\Delta/2\pi = 1.2$ THz, and $3\Omega/2\pi = 1.9$ THz, qualitatively reproducing the experimental observation in Fig. 1(d).

Finally, to understand the full time evolution of the THz 2DCS response induced by single-cycle THz pulses for different delay times τ , we modeled the time evolution of the nonlinear signal in close analogy with the previously discussed results (see Supplemental Material [56]). In particular, we modeled the largest contribution of the coherent response by a nonlinear kernel peaked at 2Δ and additionally included a phenomenological incoherent kernel describing the out-of-equilibrium quasiparticle relaxation. Figure S19(b) presents the simulated 2D spectra that qualitatively reproduces the data in Fig. S19(a) [56]. In the case of the narrow-band pulses, we can understand the THz 2D power spectra using the frequency-vector scheme [52,69], as shown in Supplemental Material [56]. It is worth mentioning that the FH signals at $\omega_\tau = \pm\Omega$ are not resolvable in the strong-pump weak-probe experiments reported previously [25], as it derives from a single pump photon and two probe photons (see Supplemental Material [56]).

In summary, we reported the THz nonlinear signal in conventional superconductors NbN using THz 2DCS. Using broadband THz pulses, we identified a prominent spectral component of the nonlinear signal peaked at twice the SC gap energy 2Δ . With narrow-band THz pulses, the same nonlinear signal appeared at the driving THz frequency Ω , in a fashion inaccessible in previous experiments. By varying the temperature, it manifests a resonant enhancement when $\Omega = 2\Delta$. General theoretical analysis showed that this resonance at $\Omega = 2\Delta$ in the nonlinear kernel can arise only from a paramagnetic coupling of photons to electronic current. Our numerical simulations revealed that this resonance in the paramagnetic nonlinear current is dominated by the amplitude mode of the SC order parameter.

Our Letter not only establishes the ability of THz 2DCS to access light-matter interactions unresolvable by previous THG or pump-probe experiments, but it also unambiguously demonstrates the intrinsic difference between the excitation processes contributing to the THz nonlinear response as compared to the optical nonlinearity that is usually understood by analogy to spontaneous nonresonant Raman spectroscopy. These results open a novel perspective on the ability of THz 2DCS to detect and/or drive other collective excitations such as the Leggett mode in multi-band superconductors [27,70], the Bardasis-Schrieffer mode in iron-based superconductors [37,71], or the Josephson plasmon in cuprate superconductors [72–78].

We acknowledge Y. Gallais, S. Houver, A.-M. Tremblay, and R. Matsunaga for discussions. This project was supported by the Gordon and Betty Moore Foundation, EPIQS initiative, Grants No. GBMF-9454 and No. NSF-DMR 2226666, by the Sapienza University under Ateneo Projects No. RM12117A4A7FD11B and

No. RP1221816662A977, and by the European Union under Grant No. ERC-SYN, MORE-TEM, GA 951215. K. K. was supported by Overseas Research Fellowship of the JSPS. N. P. A., L. B., and J. F. acknowledge the hospitality of the KITP (QUASIPART23 program), through support of NSF under Grants No. NSF PHY-1748958 and No. NSF PHY-2309135. P. R. and J. J. acknowledge the Department of Atomic Energy, Government of India (Grants No. 12-R&D-TFR-5.10-0100). G. S. acknowledges financial support from the Deutsche Forschungsgemeinschaft under SE 806/20-1.

*kk5461@nyu.edu

- [1] D. Pekker and C. M. Varma, *Annu. Rev. Condens. Matter Phys.* **6**, 269 (2015).
- [2] R. Shimano and N. Tsuji, *Annu. Rev. Condens. Matter Phys.* **11**, 103 (2020).
- [3] J. C. Tsang, J. E. Smith, and M. W. Shafer, *Phys. Rev. Lett.* **37**, 1407 (1976).
- [4] J. Demsar, K. Biljaković, and D. Mihailovic, *Phys. Rev. Lett.* **83**, 800 (1999).
- [5] S. Sugai, Y. Takayanagi, and N. Hayamizu, *Phys. Rev. Lett.* **96**, 137003 (2006).
- [6] R. Yusupov, T. Mertelj, V. V. Kabanov, S. Brazovskii, P. Kusar, J. H. Chu, I. R. Fisher, and D. Mihailovic, *Nat. Phys.* **6**, 681 (2010).
- [7] C. Rüegg, B. Normand, M. Matsumoto, A. Furrer, D. F. McMorrow, K. W. Krämer, H. U. Güdel, S. N. Gvasaliya, H. Mutka, and M. Boehm, *Phys. Rev. Lett.* **100**, 205701 (2008).
- [8] P. Merchant, B. Normand, K. Krämer, M. Boehm, D. McMorrow, and C. Rüegg, *Nat. Phys.* **10**, 373 (2014).
- [9] A. Jain, M. Krautloher, J. Porras, G. Ryu, D. Chen, D. Abernathy, J. Park, A. Ivanov, J. Chaloupka, G. Khaliullin *et al.*, *Nat. Phys.* **13**, 633 (2017).
- [10] D. M. Lee, *J. Phys. Chem. Solids* **59**, 1682 (1998).
- [11] G. Volovik and M. Zubkov, *J. Low Temp. Phys.* **175**, 486 (2014).
- [12] T. Cea, C. Castellani, and L. Benfatto, *Phys. Rev. B* **93**, 180507(R) (2016).
- [13] M. Udina, J. Fiore, T. Cea, C. Castellani, G. Seibold, and L. Benfatto, *Faraday Discuss.* **237**, 168 (2022).
- [14] L. Benfatto, C. Castellani, and T. Cea, *Phys. Rev. Lett.* **129**, 199701 (2022).
- [15] T. P. Devereaux and R. Hackl, *Rev. Mod. Phys.* **79**, 175 (2007).
- [16] R. Sooryakumar and M. V. Klein, *Phys. Rev. Lett.* **45**, 660 (1980).
- [17] P. B. Littlewood and C. M. Varma, *Phys. Rev. Lett.* **47**, 811 (1981).
- [18] P. B. Littlewood and C. M. Varma, *Phys. Rev. B* **26**, 4883 (1982).
- [19] M. A. Méasson, Y. Gallais, M. Cazayous, B. Clair, P. Rodière, L. Cario, and A. Sacuto, *Phys. Rev. B* **89**, 060503(R) (2014).
- [20] R. Grasset, T. Cea, Y. Gallais, M. Cazayous, A. Sacuto, L. Cario, L. Benfatto, and M.-A. Méasson, *Phys. Rev. B* **97**, 094502 (2018).

- [21] R. Grasset, Y. Gallais, A. Sacuto, M. Cazayous, S. Mañas Valero, E. Coronado, and M.-A. Méasson, *Phys. Rev. Lett.* **122**, 127001 (2019).
- [22] T. Cea and L. Benfatto, *Phys. Rev. B* **94**, 064512 (2016).
- [23] R. Matsunaga, N. Tsuji, H. Fujita, A. Sugioka, K. Makise, Y. Uzawa, H. Terai, Z. Wang, H. Aoki, and R. Shimano, *Science* **345**, 1145 (2014).
- [24] N. Tsuji and H. Aoki, *Phys. Rev. B* **92**, 064508 (2015).
- [25] R. Matsunaga and R. Shimano, in *Proceedings of Ultrafast Phenomena and Nanophotonics XIX* (SPIE, Bellingham, WA, 2015), Vol. 9361, pp. 150–157, [10.1117/12.2076142](https://doi.org/10.1117/12.2076142).
- [26] R. Matsunaga, N. Tsuji, K. Makise, H. Terai, H. Aoki, and R. Shimano, *Phys. Rev. B* **96**, 020505(R) (2017).
- [27] F. Giorgianni, T. Cea, C. Vicario, C.P. Hauri, W.K. Withanage, X. Xi, and L. Benfatto, *Nat. Phys.* **15**, 341 (2019).
- [28] S. Kovalev, T. Dong, L.-Y. Shi, C. Reinhoffer, T.-Q. Xu, H.-Z. Wang, Y. Wang, Z.-Z. Gan, S. Germanskiy, J.-C. Deinert, I. Ilyakov, P.H.M. van Loosdrecht, D. Wu, N.-L. Wang, J. Demsar, and Z. Wang, *Phys. Rev. B* **104**, L140505 (2021).
- [29] C. Reinhoffer, P. Pilch, A. Reinold, P. Derendorf, S. Kovalev, J.-C. Deinert, I. Ilyakov, A. Ponomaryov, M. Chen, T.-Q. Xu, Y. Wang, Z.-Z. Gan, D.-S. Wu, J.-L. Luo, S. Germanskiy, E.A. Mashkovich, P.H.M. van Loosdrecht, I.M. Eremin, and Z. Wang, *Phys. Rev. B* **106**, 214514 (2022).
- [30] K. Katsumi, N. Tsuji, Y.I. Hamada, R. Matsunaga, J. Schneeloch, R.D. Zhong, G.D. Gu, H. Aoki, Y. Gallais, and R. Shimano, *Phys. Rev. Lett.* **120**, 117001 (2018).
- [31] K. Katsumi, Z. Z. Li, H. Raffy, Y. Gallais, and R. Shimano, *Phys. Rev. B* **102**, 054510 (2020).
- [32] H. Chu *et al.*, *Nat. Commun.* **11**, 1793 (2020).
- [33] H. Chu *et al.*, *Nat. Commun.* **14**, 1343 (2023).
- [34] M.-J. Kim, S. Kovalev, M. Udina, R. Haenel, G. Kim, M. Puviani, G. Cristiani, I. Ilyakov, T. V. A. G. de Oliveira, A. Ponomaryov, J.-C. Deinert, G. Logvenov, B. Keimer, D. Manske, L. Benfatto, and S. Kaiser, *Sci. Adv.* **10**, eadi7598 (2024).
- [35] C. Vaswani, J.H. Kang, M. Mootz, L. Luo, X. Yang, C. Sundahl, D. Cheng, C. Huang, R.H.J. Kim, Z. Liu, Y.G. Collantes, E.E. Hellstrom, I.E. Perakis, C.B. Eom, and J. Wang, *Nat. Commun.* **12**, 258 (2021).
- [36] K. Isoyama, N. Yoshikawa, K. Katsumi, J. Wong, N. Shikama, Y. Sakishita, F. Nabeshima, A. Maeda, and R. Shimano, *Commun. Phys.* **4**, 160 (2021).
- [37] R. Grasset, K. Katsumi, P. Massat, H.-H. Wen, X.-H. Chen, Y. Gallais, and R. Shimano, *npj Quantum Mater.* **7**, 4 (2022).
- [38] L. Luo, M. Mootz, J.H. Kang, C. Huang, K. Eom, J. W. Lee, C. Vaswani, Y.G. Collantes, E.E. Hellstrom, I.E. Perakis, C.B. Eom, and J. Wang, *Nat. Phys.* **19**, 201 (2023).
- [39] M. Mootz, L. Luo, J. Wang, and I.E. Perakis, *Commun. Phys.* **5**, 47 (2022).
- [40] T. Jujo, *J. Phys. Soc. Jpn.* **87**, 024704 (2018).
- [41] Y. Murotani and R. Shimano, *Phys. Rev. B* **99**, 224510 (2019).
- [42] M. Silaev, *Phys. Rev. B* **99**, 224511 (2019).
- [43] N. Tsuji and Y. Nomura, *Phys. Rev. Res.* **2**, 043029 (2020).
- [44] G. Seibold, M. Udina, C. Castellani, and L. Benfatto, *Phys. Rev. B* **103**, 014512 (2021).
- [45] J. Fiore, M. Udina, M. Marciani, G. Seibold, and L. Benfatto, *Phys. Rev. B* **106**, 094515 (2022).
- [46] G. Seibold, *Condens. Matter* **8**, 95 (2023).
- [47] M. Puviani, R. Haenel, and D. Manske, *Phys. Rev. B* **107**, 094501 (2023).
- [48] S. T. Cundiff and S. Mukamel, *Phys. Today* **66**, No. 7, 44 (2013).
- [49] J. Lu, X. Li, H. Y. Hwang, B. K. Ofori-Okai, T. Kurihara, T. Suemoto, and K. A. Nelson, *Phys. Rev. Lett.* **118**, 207204 (2017).
- [50] G. Folin, K. Reimann, M. Woerner, T. Elsaesser, J. Hoja, and A. Tkatchenko, *Phys. Rev. Lett.* **119**, 097404 (2017).
- [51] S. Houver, L. Huber, M. Savoini, E. Abreu, and S.L. Johnson, *Opt. Express* **27**, 10854 (2019).
- [52] F. Mahmood, D. Chaudhuri, S. Gopalakrishnan, R. Nandkishore, and N. P. Armitage, *Nat. Phys.* **17**, 627 (2021).
- [53] J. Hebling, G. Almasi, I. Kozma, and J. Kuhl, *Opt. Express* **10**, 1161 (2002).
- [54] S. Watanabe, N. Minami, and R. Shimano, *Opt. Express* **19**, 1528 (2011).
- [55] H. Hirori, A. Doi, F. Blanchard, and K. Tanaka, *Appl. Phys. Lett.* **98**, 091106 (2011).
- [56] See Supplemental Material at <http://link.aps.org/supplemental/10.1103/PhysRevLett.132.256903> for the details of the experimental setup, equilibrium optical properties of the samples, the additional THz 2DCS data, theoretical analysis, and numerical simulations, which includes Refs. [57–64].
- [57] S. P. Chockalingam, M. Chand, J. Jesudasan, V. Tripathi, and P. Raychaudhuri, *Phys. Rev. B* **77**, 214503 (2008).
- [58] D. Chaudhuri, D. Barbalas, R. Romero III, F. Mahmood, J. Liang, J. Jesudasan, P. Raychaudhuri, and N. P. Armitage, [arXiv:2204.04203](https://arxiv.org/abs/2204.04203).
- [59] W. Zimmermann, E. Brandt, M. Bauer, E. Seider, and L. Genzel, *Physica (Amsterdam)* **183C**, 99 (1991).
- [60] D. C. Mattis and J. Bardeen, *Phys. Rev.* **111**, 412 (1958).
- [61] Y. Ikebe, R. Shimano, M. Ikeda, T. Fukumura, and M. Kawasaki, *Phys. Rev. B* **79**, 174525 (2009).
- [62] L. Benfatto, C. Castellani, and G. Seibold, *Phys. Rev. B* **108**, 134508 (2023).
- [63] M. Udina, T. Cea, and L. Benfatto, *Phys. Rev. B* **100**, 165131 (2019).
- [64] R. Matsunaga and R. Shimano, *Phys. Rev. Lett.* **109**, 187002 (2012).
- [65] R. W. Boyd, *Nonlinear Optics*, 3rd ed. (Academic, New York, 2008).
- [66] T. E. Glier, M. Rerrer, L. Westphal, G. Lüllau, L. Feng, S. Tian, J. Dolgner, R. Haenel, M. Zonno, H. Eisaki, M. Greven, A. Damascelli, S. Kaiser, D. Manske, and M. Rübhausen, [arXiv:2310.08162](https://arxiv.org/abs/2310.08162).
- [67] M. Chand, Transport, magneto-transport and electron tunneling studies on disordered superconductors, Ph.D. thesis, Tata Institute of Fundamental Research, 2012.
- [68] B. Cheng, L. Wu, N.J. Laurita, H. Singh, M. Chand, P. Raychaudhuri, and N. P. Armitage, *Phys. Rev. B* **93**, 180511(R) (2016).
- [69] M. Woerner, W. Kuehn, P. Bowlan, K. Reimann, and T. Elsaesser, *New J. Phys.* **15**, 025039 (2013).

- [70] G. Blumberg, A. Mialitsin, B. S. Dennis, M. V. Klein, N. D. Zhigadlo, and J. Karpinski, *Phys. Rev. Lett.* **99**, 227002 (2007).
- [71] F. Kretzschmar, B. Muschler, T. Böhm, A. Baum, R. Hackl, H.-H. Wen, V. Tsurkan, J. Deisenhofer, and A. Loidl, *Phys. Rev. Lett.* **110**, 187002 (2013).
- [72] S. Rajasekaran, E. Casandruc, Y. Laplace, D. Nicoletti, G. D. Gu, S. R. Clark, D. Jaksch, and A. Cavalleri, *Nat. Phys.* **12**, 1012 (2016).
- [73] S. Rajasekaran, J. Okamoto, L. Mathey, M. Fechner, V. Thampy, G. D. Gu, and A. Cavalleri, *Science* **359**, 575 (2018).
- [74] F. Gabriele, M. Udina, and L. Benfatto, *Nat. Commun.* **12**, 752 (2021).
- [75] S. J. Zhang, Q. M. Liu, Z. Sun, Z. X. Wang, Q. Wu, L. Yue, S. X. Xu, T. C. Hu, R. S. Li, X. Y. Zhou, J. Y. Yuan, G. D. Gu, T. Dong, and N. L. Wang, *Natl. Sci. Rev.* **10**, nwad163 (2023).
- [76] K. Kaj, K. A. Cremin, I. Hammock, J. Schalch, D. N. Basov, and R. D. Averitt, *Phys. Rev. B* **107**, L140504 (2023).
- [77] K. Katsumi, M. Nishida, S. Kaiser, S. Miyasaka, S. Tajima, and R. Shimano, *Phys. Rev. B* **107**, 214506 (2023).
- [78] A. Liu, D. Pavicevic, M. H. Michael, A. G. Salvador, P. E. Dolgirev, M. Fechner, A. S. Disa, P. M. Lozano, Q. Li, G. D. Gu, E. Demler, and A. Cavalleri, [arXiv:2308.14849](https://arxiv.org/abs/2308.14849).